ScienceAdvances

RESEARCH ARTICLES

Cite as: F. Liu *et al.*, *Sci. Adv* 10.1126/sciadv.abc2992 (2020).

Abrupt decline in tropospheric nitrogen dioxide over China after the outbreak of COVID-19

Fei Liu[1,2*], Aaron Page[3], Sarah A. Strode[1,2], Yasuko Yoshida[2,4], Sungyeon Choi[2,4], Bo Zheng[5], Lok N. Lamsal[1,2], Can Li[2,6], Nickolay A. Krotkov[2], Henk Eskes[7], Ronald van der A[7,8], Pepijn Veefkind[7,9], Pieternel F. Levelt[7,9], Oliver P. Hauser[10†], Joanna Joiner[2†]

[1]Universities Space Research Association (USRA), Columbia, MD 21046, USA. [2]NASA Goddard Space Flight Center Laboratory for Atmospheric Chemistry and Dynamics Laboratory, Greenbelt, MD 20771, USA. [3]Department of Management, University of Exeter, Exeter EX4 4PU, UK. [4]Science Systems and Applications, Inc., Lanham, MD 20706, USA. [5]Laboratoire des Sciences du Climat et de l'Environnement, CEA-CNRS-UVSQ, Gif-sur-Yvette, UMR 8212, France. [6]Earth System Science Interdisciplinary Center, University of Maryland, College Park, MD 20740, USA. [7]Royal Netherlands Meteorological Institute (KNMI), De Bilt 3731 GA, The Netherlands. [8]Nanjing University of Information Science & Technology (NUIST), No.219, Ningliu Road, Nanjing, Jiangsu, P.R.China. [9]Delft University of Technology, Delft 2628 CD, The Netherlands. [10]Department of Economics, University of Exeter, Exeter EX4 4PU, UK.

*Corresponding author. Email: fliu@usra.edu †Contributed equally

China's policy interventions to reduce the spread of the coronavirus disease 2019 have environmental and economic impacts. Tropospheric nitrogen dioxide indicates economic activities, as nitrogen dioxide is primarily emitted from fossil fuel consumption. Satellite measurements show a 48% drop in tropospheric nitrogen dioxide vertical column densities from the 20 days averaged before the 2020 Lunar New Year to the 20 days averaged after. This is 21% ± 5% larger than that from 2015–2019. We relate this reduction to two of the government's actions: the announcement of the first report in each province and the date of a province's lockdown. Both actions are associated with nearly the same magnitude of reductions. Our analysis offers insights into the unintended environmental and economic consequences through reduced economic activities.

Introduction

In December 2019, a respiratory disease, coronavirus disease 2019 (COVID-19), emerged in Wuhan City, Hubei Province, China (*1*). COVID-19 has since spread worldwide causing tens of thousands of deaths (*2*). To combat the spread of COVID-19, the Chinese government sealed off several cities reporting large numbers of infected people, including Wuhan, starting January 23, 2020; this included halting public transportation and closing local businesses. These prevention efforts quickly expanded nationwide. The policy announcements and restrictions, applied at an unprecedented scale, have implications for the Chinese environment and the economy that we quantitatively evaluate in this paper. In particular, we use satellite nitrogen dioxide (NO_2) measurements to monitor changes in fossil fuel usage, related to economic activity, over China following the outbreak of COVID-2019. Nitrogen oxides ($NO + NO_2 = NO_x$), emitted during high temperature combustion, are relatively short-lived in the atmosphere (lifetimes of the order of hours near the surface), and therefore remain relatively close to their sources (*3*). NO_2 tropospheric vertical column density (TVCD) retrieved from backscattered solar radiation, such as from the Ozone Monitoring Instrument (OMI) (*4*), has been widely used to monitor both long term and short-term changes in fuel consumption (*5, 6*). OMI's successor, the Tropospheric Monitoring Instrument (TROPOMI) (*7*) offers a higher spatial resolution measurement of NO_2 TVCD.

Results and Discussion

We observe substantial reductions of NO_2 TVCD after the 2020 Lunar New Year (LNY) on January 25, 2020. Fig. 1 shows 20-day averages of OMI NO_2 TVCD before, during and after the 2020 LNY (hereafter referred to as the "pre", "peri" and "post" periods). An average reduction of 48% in NO_2 TVCD over China is observed from pre to peri periods. Consistency in the trends of retrieved NO_2 TVCD is found between OMI and its successor TROPOMI (Figure S1). A reduction in NO_2 TVCD is typically observed during LNY because most Chinese factories shut down for the holiday and the traffic volumes decrease, resulting in a decrease in fuel consumption and thus NO_x emissions. OMI NO_2 TVCD shows a pre to peri decline of 27% ± 5% (mean ± standard deviation) from data covering the 2015 to 2019 period (Fig. S2). Similarly, TROPOMI shows a reduction of 33% in 2019 (Fig. S3). This suggests that the observed reduction in 2020 far exceeds (21% ± 5%) the typical holiday-related pre to peri period reduction.

Consistent with the 2015–2019 data, the 2020 NO_2 TVCD 7-day moving averages show a significant reduction during approximately the two weeks leading up to LNY and reach a minimum around LNY, consistent with the gradual shutdown of factories before the holiday (Fig. 2). In prior years, a

rebound of NO_2 TVCD usually begins around 7 days after LNY, marking the end of the holiday season. OMI and TROPOMI (Fig. S4) NO_2 TVCDs show similar temporal patterns prior to 2020 with a clear reduction before LNY and an increase shortly thereafter. However, while the 2020 data show similar initial declines in the week leading up to LNY, we do not observe the typical uptick in NO_2 TVCDs starting the week after the LNY as in previous years (Fig. 2). OMI (and TROPOMI) NO_2 TVCDs show a longer period of low values near the minimum. Note that the 2020 data are generally lower than previous years, probably reflecting in part the effects of China's clean air policies that require installation of denitrification devices for all coal-fired power plants and cement plants (*8*).

To rule out the possibility that the large NO_2 TVCD decreases observed in 2020 may be driven by changes in the meteorological conditions affecting local NO_x chemistry and NO_x transport, we use Goddard Earth Observing System coupled to the NASA Global Modeling Initiative (GEOS-GMI) (*9*) model simulations with constant emissions. We find the simulated effects of meteorology on NO_2 TVCD small as compared with the prolonged NO_2 reduction we observe from the pre to peri period (Fig. S5). The simulation with constant emissions shows many areas with increases from the pre to peri periods (Fig. S6). This suggests that in many areas the actual decrease in NO_x emissions may be larger than what is inferred from the observed NO_2 TVCDs.

Breaking these results down by sectors provides insights into the sources of reduction. All sectors experienced dramatic NO_2 reductions. We compute 7-day running averages for all OMI observations within 0.25° gridboxes that contain large power plants or other industrial plants with reported NO_x emissions > 5 Gg/yr (Fig. S7). OMI NO_2 TVCD averages for gridboxes containing power plants and those for other industrial plants show similar temporal variations as the national average (Fig. S8). This suggests that measures to reduce COVID-19 spread affected power generation as well as industrial production including steel, iron, and oil. Direct NO_2 reductions from transportation are indicated by the visually reduced TROPOMI NO_2 TVCDs along the China National Highways (Fig. 3).

We next explore how COVID-19 policy interventions (most of which happened to coincide with the 2020 LNY) are associated with reductions in NO_2 TVCD. First, we consider the announcements the government made to the public (Table S1). Once the government publicly reports that a COVID-19 case has been confirmed in a province, the public in that province might choose to reduce their exposure to others (e.g., stay at home, work from home and/or travel less). In that case, we would expect a reduction in NO_2 TVCD following the announcement of the first case in each province. This is indeed what we find, after taking previous years' NO_2 TVCD and variation across provinces into account (see Eq. 1): following the report of the first case in each province, OMI NO_2 TVCD declined by about 27% (coeff = -1.383, p = 0.002, Table 1 Col. 1).

The second policy intervention is more invasive: the government took decisive action to further reduce the spread of the virus by limiting the mobility of citizens and locking down entire provinces; on average, lockdowns occurred 3.7 days after the report of the first case. We would expect that a lockdown would be followed by a reduction in travel as well as business activity, which in turn should lead to reductions of NO_2 TVCD. Our model (Eq. 2) shows that OMI NO_2 TVCD reduces by 24% following the lockdowns (coeff = -1.134, p < 0.001, Table 1 Col. 2).

Finally, we consider the two policies jointly (Eq. 3). We find that both the announcement of the first case reported as well as the lockdown are associated with a reduction in NO_2 TVCDs in each province (Table 1 Col. 3). These results suggest that the effect of the announcement is about as large (16%; coeff = -0.851, p = 0.043) as the effect of the lockdown (15%; coeff = -0.752, p < 0.001). All results are qualitatively similar using TROPOMI (Table S2).

NO_2 reductions are closely related to improvements in air quality (*10*). Under normal circumstances, many Chinese cities have poor air quality that reduces life quality and expectancy (*11*). During the COVID-19 crisis, NO_2 pollution was additionally reduced by ~20% for a period of between 30 and 50 days. While temporary, these substantial reductions in air pollution may have positive health impact for lives in otherwise heavily polluted areas (*12*). This unusual period offers a rare counterfactual of a potential society which uses substantially less fossil fuels and has lower mobility (*13*).

While this research provides an early insight into the NO_2 changes in China in early 2020, our findings are not without limitations. Because the relationship between NO_2 TVCD and NO_x emissions is not strictly linear, the analysis of NO_2 TVCD provides a qualitative description of changes in NO_x emissions. Accurately quantifying the changes in NO_x emissions (*14*) is beyond the scope of this initial assessment.

Our results suggest that the announcement of the first case was followed by a reduction in NO_2 emissions, with a further reduction following the actual lockdown. However, it is important to note that these results do not suggest that the mobility restrictions did not have a critical impact. Indeed, recently published work suggests that the travel restrictions in China reduced the spread of the disease by up to 80% by mid-February, in particular internationally (*15*). In line with our results is the finding that human mobility was reduced early on during the outbreak (*16*) and may in part have started as early as the first case announcements, with additional reductions through lockdowns.

Materials and Methods

Satellite NO_2 observations

We use retrieved NO_2 TVCD from both OMI and TROPOMI. OMI is a Dutch-Finnish UV-VIS spectrometer (*4*) on board the US National Aeronautics and Space Administration (NASA) Aura satellite that was launched in 2004. TROPOMI is a UV-VIS-NIR-SWIR instrument (*7*) on board the European Copernicus Sentinel-5 Precursor satellite that was launched in 2017. Both instruments similarly measure Earth radiance and solar irradiance spectra with spectral resolutions of approximately 0.5 nm. The ratio of radiance to irradiance at wavelengths between 400 and 496 nm is used to retrieve NO_2 TVCD. The ground footprint sizes are 13×24 km^2 and 3.5×5.5 km^2 (3.5×7 km^2 before August, 2019) at nadir for OMI and TROPOMI, respectively. Both instruments provide nearly daily to bi-daily global coverage with a local equator crossing times close to 13:30 hours. We use the version 4.0 NASA OMI standard NO_2 products (*17*). We use the version 1.0.0 TROPOMI Level 2 offline NO_2 data products for 2019 and the version 1.1.0 data for 2020 (*18*). OMI and TROPOMI measurements are aggregated to resolutions of 0.25°×0.25° and 0.05°×0.05°, respectively. A given gridbox value is computed by averaging the pixel-level satellite observations weighted by the amount of the pixel footprint that overlaps the gridbox. We remove OMI observations with effective cloud fractions >30% to reduce retrieval errors and those affected by the so-called "row anomaly" (*19*). For TROPOMI, we use only observations with quality assurance values > 0.75.

For the maps shown, we calculate 20-day means of NO_2 TVCD around the Lunar New Year using OMI during 2015–2020 and TROPOMI for 2019 and 2020. We only include regions dominated by anthropogenic NO_x emissions in the analysis; these are defined as regions with average annual OMI NO_2 TVCDs > 1×10^{15} molec/cm^2 over the period of 2005–2019 (Fig S7) (*20*). For time series analysis, we further compute 7-day running averages to smooth out daily fluctuations in NO_2 TVCD due to retrieval noise, including the effects of clouds, and influences of meteorology (wind-driven transport influences NO_2 TVCDs).

Sector information

We select facilities with reported NO_x emissions > 5 Gg/yr (*21*). The locations of 245 heavy industry plants including steel, iron, coke, oil, cement and glass industry, and 103 power plants considered in this analysis are shown in Figure S7. We compute 7-day running averages of OMI NO_2 TVCD for gridboxes where large power plants and other industrial plants are located for 2020 ($TVCD_{2020}$) and the mean of 2015–2019 ($TVCD_{\overline{2015-2019}}$). We calculate the relative difference as $(TVCD_{2020} - TVCD_{\overline{2015-2019}})/TVCD_{\overline{2015-2019}}$.

GEOS-GMI NO_2 simulations

We ran the GEOS-GMI (*9*) with anthropogenic and biomass burning emissions of NO_x and other trace gas emissions held constant to simulate NO_2 TVCD over China in order to estimate the potential impact of meteorology on NO_2 TVCDs from January to February, 2020. The simulation uses the Global Modeling Initiative (GMI) chemistry mechanism (*22*) and the Goddard Chemistry Aerosol Radiation and Transport component of GEOS-5 (*23, 24*) to interact with the GMI chemistry. The simulation's meteorology is constrained by the Modern-Era Retrospective analysis for Research and Applications, Version 2 (MERRA2) (*25*) assimilated meteorological data from the NASA Global Modeling and Assimilation Office (GMAO) GEOS-5 data assimilation system. The constant anthropogenic emissions are from the Representative Concentration Pathways (RCP) 6.0 scenario (*26*) for January 2019, downscaled to higher resolution using the Emissions Database for Global Atmospheric Research (EDGAR) version 4.3.2 (*27*) inventory. Constant biomass burning emissions are the January 2020 monthly mean from the Quick Fire Emissions Dataset version 2 (QFED2) (*28*). This simulation includes 72 vertical levels at a spatial resolution of 0.25° (latitude and longitude) and a model time step of 7.5 min. We sample the model output only when and where there are valid satellite observations.

Statistical analysis of policy responses

For the policy evaluation, we make use of the timing of when the Chinese government first publicly reported that a person was infected with COVID-19, which occurred on several different dates across the country's provinces. The first public announcement of "viral pneumonia of unknown cause" in Wuhan occurred on January 3, 2020. Daily public health statements began on January 11, 2020, which included the new cases, deaths, and recoveries reported separately for each province. Of particular interest for our analysis are the times when the government announced the first case in *each* province (Table S1). We also use the exact timing when the government put restrictive mobility policies in place, in order to reduce the likelihood of transmission. The first such policy was put in place for Wuhan on January 23, 2020, followed by more restrictions for other provinces shortly after (Table S1).

We conduct a statistical evaluation of the exact timing of the reduction in NO_2 TVCDs. While the 2020 Lunar New Year coincided roughly with the lockdown of most Chinese provinces, the government's policy actions actually took two forms and varied over time. The first policy action was public announcements of new cases in each province, while the second policy action was to restrict movement and order citizens to stay in-doors (which became known as "lockdown"). We explore the timing of these two potential candidates—announcements of new cases and restrictive mobility policies—

to identify to what extent they are responsible for NO_2 TVCD reductions. We take advantage of the temporal variation of these measures across the country.

To analyze the effects of these policies, we use fixed-effects models that predict tropospheric NO_2 TVCD, controlling for previous years' NO_2 TVCD as well as fixed effects for each province:

$$z_{t,p} = \alpha + \beta x_{t,p} + \delta z_{prior} + v_p + \varepsilon_{t,p} \qquad (1)$$

where z is the outcome variable (daily NO_2 TVCD for the period from 4 weeks before LNY to 8 weeks after LNY), x is an indicator variable on and after the first case is announced on day t in province p (which remains 1 after the first case; otherwise coded as 0), z_{prior} is the NO_2 TVCD in prior years (which is the average of years 2015 and 2019 for the OMI data and of the year 2019 for the TROPOMI data where prior data are only available for 2019), α is the average fixed effect across all provinces and v is the fixed effect of province p (relative to α), and ε is an error term that is clustered at the province p.

To estimate the effect of the lockdown policy, we use the following fixed-effects model:

$$z_{t,p} = \alpha + \lambda y_{t,p} + \delta z_{prior} + v_p + \varepsilon_{t,p} \qquad (2)$$

where y is an indicator variable for the lockdown of the province p starting on day t (which is 1 during the time of the lockdown; otherwise coded as 0), and all other variables are as defined above.

We use a similar fixed-effects model predicting the effect of both policies jointly:

$$z_{t,p} = \alpha + \beta x_{t,p} + \lambda y_{t,p} + \delta z_{prior} + v_p + \varepsilon_{t,p} \qquad (3)$$

where all variables are as previously specified. β, λ and δ are the derived coefficients of the model.

Using the above specified fixed-effect models enables us to estimate the effect of the policy precisely, as we hold constant province-specific variation as well as prior year variation in NO_2. Our primary analysis uses OMI data (Table 1) but our results are qualitatively unchanged if we use TROPOMI data (Table S2).

REFERENCES AND NOTES

1. C. Huang, Y. Wang, X. Li, L. Ren, J. Zhao, Y. Hu, L. Zhang, G. Fan, J. Xu, X. Gu, Z. Cheng, T. Yu, J. Xia, Y. Wei, W. Wu, X. Xie, W. Yin, H. Li, M. Liu, Y. Xiao, H. Gao, L. Guo, J. Xie, G. Wang, R. Jiang, Z. Gao, Q. Jin, J. Wang, B. Cao, Clinical features of patients infected with 2019 novel coronavirus in Wuhan, China. *Lancet* **395**, 497–506 (2020). doi:10.1016/S0140-6736(20)30183-5 Medline
2. E. Dong, H. Du, L. Gardner, An interactive web-based dashboard to track COVID-19 in real time. *Lancet Infect. Dis.* **20**, 533–534 (2020). doi:10.1016/S1473-3099(20)30120-1 Medline
3. J. H. Seinfeld, S. N. Pandis, *Atmospheric chemistry and physics: From air pollution to climate change.* (John Wiley and Sons, New York, ed. 2, 2006), pp. 204–275.
4. P. F. Levelt, J. Joiner, J. Tamminen, J. P. Veefkind, P. K. Bhartia, D. C. Stein Zweers, B. N. Duncan, D. G. Streets, H. Eskes, R. van der A, C. McLinden, V. Fioletov, S. Carn, J. de Laat, M. DeLand, S. Marchenko, R. McPeters, J. Ziemke, D. Fu, X. Liu, K. Pickering, A. Apituley, G. González Abad, A. Arola, F. Boersma, C. Chan Miller, K. Chance, M. de Graaf, J. Hakkarainen, S. Hassinen, I. Ialongo, Q. Kleipool, N. Krotkov, C. Li, L. Lamsal, P. Newman, C. Nowlan, R. Suleiman, L. G. Tilstra, O. Torres, H. Wang, K. Wargan, R. van der A, C. McLinden, V. Fioletov, S. Carn, J. de Laat, M. DeLand, S. Marchenko, R. McPeters, J. Ziemke, D. Fu, X. Liu, K. Pickering, A. Apituley, G. González Abad, A. Arola, F. Boersma, C. Chan Miller, K. Chance, M. de Graaf, J. Hakkarainen, S. Hassinen, I. Ialongo, Q. Kleipool, N. Krotkov, C. Li, L. Lamsal, P. Newman, C. Nowlan, R. Suleiman, L. G. Tilstra, O. Torres, H. Wang, K. Wargan, The Ozone Monitoring Instrument: Overview of 14 years in space. *Atmos. Chem. Phys.* **18**, 5699–5745 (2018). doi:10.5194/acp-18-5699-2018
5. B. N. Duncan, L. N. Lamsal, A. M. Thompson, Y. Yoshida, Z. Lu, D. G. Streets, M. M. Hurwitz, K. E. Pickering, A space-based, high-resolution view of notable changes in urban NO_x pollution around the world (2005–2014). *J. Geophys. Res.* **121**, 976–996 (2016).
6. B. Mijling, R. J. van der A, K. F. Boersma, M. Van Roozendael, I. De Smedt, H. M. Kelder, R. J. van der A, K. F. Boersma, M. Van Roozendael, I. De Smedt, H. M. Kelder, Reductions of NO_2 detected from space during the 2008 Beijing Olympic Games. *Geophys. Res. Lett.* **36**, L13801 (2009). doi:10.1029/2009GL038943
7. J. P. Veefkind, I. Aben, K. McMullan, H. Förster, J. de Vries, G. Otter, J. Claas, H. J. Eskes, J. F. de Haan, Q. Kleipool, M. van Weele, O. Hasekamp, R. Hoogeveen, J. Landgraf, R. Snel, P. Tol, P. Ingmann, R. Voors, B. Kruizinga, R. Vink, H. Visser, P. F. Levelt, TROPOMI on the ESA Sentinel-5 Precursor: A GMES mission for global observations of the atmospheric composition for climate, air quality and ozone layer applications. *Remote Sens. Environ.* **120**, 70–83 (2012). doi:10.1016/j.rse.2011.09.027
8. R. Wu, F. Liu, D. Tong, Y. Zheng, Y. Lei, C. Hong, M. Li, J. Liu, B. Zheng, Y. Bo, X. Chen, X. Li, Q. Zhang, Air quality and health benefits of China's emission control policies on coal-fired power plants during 2005–2020. *Environ. Res. Lett.* **14**, 094016 (2019). doi:10.1088/1748-9326/ab3bae
9. S. A. Strode, J. R. Ziemke, L. D. Oman, L. N. Lamsal, M. A. Olsen, J. Liu, Global changes in the diurnal cycle of surface ozone. *Atmos. Environ.* **199**, 323–333 (2019). doi:10.1016/j.atmosenv.2018.11.028
10. J. L. Laughner, R. C. Cohen, Direct observation of changing NO_x lifetime in North American cities. *Science* **366**, 723–727 (2019). doi:10.1126/science.aax6832 Medline
11. A. Ebenstein, M. Fan, M. Greenstone, G. He, P. Yin, M. Zhou, Growth, Pollution, and Life Expectancy: China from 1991–2012. *Am. Econ. Rev.* **105**, 226–231 (2015). doi:10.1257/aer.p20151094
12. M. Burke, COVID-19 reduces economic activity, which reduces pollution, which saves lives. Available at www.g-feed.com/2020/03/covid-19-reduces-economic-activity.html (last access: 2020-03-28)
13. N. Obradovich, I. Rahwan, Risk of a feedback loop between climatic warming and human mobility. *J. R. Soc. Interface* **16**, 20190058 (2019). doi:10.1098/rsif.2019.0058 Medline
14. L. N. Lamsal, R. V. Martin, A. Padmanabhan, A. van Donkelaar, Q. Zhang, C. E. Sioris, K. Chance, T. P. Kurosu, M. J. Newchurch, Application of satellite observations for timely updates to global anthropogenic NO_x emission inventories. *Geophys. Res. Lett.* **38**, L05810 (2011). doi:10.1029/2010GL046476
15. M. Chinazzi, J. T. Davis, M. Ajelli, C. Gioannini, M. Litvinova, S. Merler, A. Pastore Y Piontti, K. Mu, L. Rossi, K. Sun, C. Viboud, X. Xiong, H. Yu, M. E. Halloran, I. M. Longini Jr., A. Vespignani, The effect of travel restrictions on the spread of the 2019 novel coronavirus (COVID-19) outbreak. *Science* **368**, 395–400 (2020). doi:10.1126/science.aba9757 Medline
16. M. U. G. Kraemer, C. H. Yang, B. Gutierrez, C. H. Wu, B. Klein, D. M. Pigott, L. du Plessis, N. R. Faria, R. Li, W. P. Hanage, J. S. Brownstein, M. Layan, A. Vespignani, H. Tian, C. Dye, O. G. Pybus, S. V. Scarpino; Open COVID-19 Data Working Group, The effect of human mobility and control measures on the COVID-19 epidemic in China. *Science* **368**, 493–497 (2020). doi:10.1126/science.abb4218 Medline
17. N. A. Krotkov, L. N. Lamsal, S. V. Marchenko, E. A. Celarier, E. J. Bucsela, W. H. Swartz, J. Joiner and the OMI core team, OMI/Aura nitrogen dioxide (NO_2) total and tropospheric column 1-orbit L2 swath 13×24 km V003. (Goddard Earth Sciences Data and Information Services Center, Greenbelt, MD, USA, 2019). Avaialbe at 10.5067/Aura/OMI/DATA2017 (last access: 2020-03-29).
18. J. van Geffen, K. F. Boersma, H. Eskes, M. Sneep, M. ter Linden, M. Zara, J. P. Veefkind, S5P TROPOMI NO_2 slant column retrieval: Method, stability, uncertainties and comparisons with OMI. *Atmos. Meas. Tech.* **13**, 1315–1335 (2020). doi:10.5194/amt-13-1315-2020
19. V. M. E. Schenkeveld, G. Jaross, S. Marchenko, D. Haffner, Q. L. Kleipool, N. C.

Rozemeijer, J. P. Veefkind, P. F. Levelt, In-flight performance of the Ozone Monitoring Instrument. *Atmos. Meas. Tech.* **10**, 1957–1986 (2017). doi:10.5194/amt-10-1957-2017 Medline
20. F. Liu, Q. Zhang, R.J. van der A, B. Zheng, D. Tong, L. Yan, Y. Zheng, K. He, Recent reduction in NO_x emissions over China: Synthesis of satellite observations and emission inventories. *Environ. Res. Lett.* **11**, 114002 (2016). doi:10.1088/1748-9326/11/11/114002
21. B. Zheng, D. Tong, M. Li, F. Liu, C. Hong, G. Geng, H. Li, X. Li, L. Peng, J. Qi, L. Yan, Y. Zhang, H. Zhao, Y. Zheng, K. He, Q. Zhang, Trends in China's anthropogenic emissions since 2010 as the consequence of clean air actions. *Atmos. Chem. Phys.* **18**, 14095–14111 (2018). doi:10.5194/acp-18-14095-2018
22. B. N. Duncan, S. E. Strahan, Y. Yoshida, S. D. Steenrod, N. Livesey, Model study of the cross-tropopause transport of biomass burning pollution. *Atmos. Chem. Phys.* **7**, 3713–3736 (2007). doi:10.5194/acp-7-3713-2007
23. M. Chin, P. Ginoux, S. Kinne, O. Torres, B. N. Holben, B. N. Duncan, R. V. Martin, J. A. Logan, A. Higurashi, T. Nakajima, Tropospheric aerosol optical thickness from the GOCART model and comparisons with satellite and sun photometer measurements. *J. Atmos. Sci.* **59**, 461–483 (2002). doi:10.1175/1520-0469(2002)059<0461:TAOTFT>2.0.CO;2
24. P. Colarco, A. da Silva, M. Chin, T. Diehl, Online simulations of global aerosol distributions in the NASA GEOS-4 model and comparisons to satellite and ground-based aerosol optical depth. *J. Geophys. Res.* **115** (D14), D14207 (2010). doi:10.1029/2009JD012820
25. R. Gelaro, W. McCarty, M. J. Suárez, R. Todling, A. Molod, L. Takacs, C. Randles, A. Darmenov, M. G. Bosilovich, R. Reichle, K. Wargan, L. Coy, R. Cullather, C. Draper, S. Akella, V. Buchard, A. Conaty, A. da Silva, W. Gu, G.-K. Kim, R. Koster, R. Lucchesi, D. Merkova, J. E. Nielsen, G. Partyka, S. Pawson, W. Putman, M. Rienecker, S. D. Schubert, M. Sienkiewicz, B. Zhao, The Modern-Era Retrospective Analysis for Research and Applications, Version 2 (MERRA-2). *J. Clim.* **30**, 5419–5454 (2017). doi:10.1175/JCLI-D-16-0758.1 Medline
26. D. P. van Vuuren, J. Edmonds, M. Kainuma, K. Riahi, A. Thomson, K. Hibbard, G. C. Hurtt, T. Kram, V. Krey, J.-F. Lamarque, T. Masui, M. Meinshausen, N. Nakicenovic, S. J. Smith, S. K. Rose, The representative concentration pathways: An overview. *Clim. Change* **109**, 5–31 (2011). doi:10.1007/s10584-011-0148-z
27. M. Crippa, D. Guizzardi, M. Muntean, E. Schaaf, F. Dentener, J. A. van Aardenne, S. Monni, U. Doering, J. G. J. Olivier, V. Pagliari, G. Janssens-Maenhout, Gridded emissions of air pollutants for the period 1970–2012 within EDGAR v4.3.2. *Earth Syst. Sci. Data* **10**, 1987–2013 (2018). doi:10.5194/essd-10-1987-2018
28. A. S. Darmenov, A. M. da Silva, The Quick Fire Emissions Dataset (QFED): Documentation of Versions 2.1, 2.2 and 2.4. R. D. Koster, Ed., *NASA Technical Report Series on Global Modeling and Data Assimilation* (2015), vol. 38, pp. 212.

ACKNOWLEDGMENTS

The authors thank the algorithm, processing, and distribution teams for the OMI and TROPOMI data sets used here. The authors thank Dr. Luke Oman for helping to set up the GEOS-GMI model runs and emissions. **Funding:** Funding for this work was provided in part by NASA through the Aura project data analysis program, and the ACMAP and the MAP program managed by Ken Jucks, Barry Lefer, and Richard Eckman, who the authors acknowledge for their continued support. **Author contributions:** Conceptualization and Methodology: F. L., A. P., J. J., O. P. H.; Formal Analysis: F. L., A. P., O. P. H.; Investigation: all; Writing – Original Draft: F. L., O. P. H., Writing – Review and Editing: all; Visualization: F. L., Supervision, Project Administration, Funding acquisition: F. L., O. P. H., J. J.; Data Curation: B. Z., L. L., C. L., N. K., H. E., R. A., P. V., P. L.; Software: F. L., A. P., Y. Y., S. C., S. S., O. P. H.. **Competing interests:** The authors declare that they have no competing interests. **Data and materials availability:** All satellite data used in this work is publicly available through NASA Goddard Earth Sciences Data and Information Services Center (https://disc.gsfc.nasa.gov/) and ESA Sentinel-5P Pre-Operations Data Hub (https://s5phub.copernicus.eu/). GMI model output and policy response data are available upon request from the authors as is code to process all data sets. All data needed to evaluate the conclusions in the paper are present in the paper and/or the Supplementary Materials. Additional data available from authors upon request.

SUPPLEMENTARY MATERIALS

advances.sciencemag.org/cgi/content/full/sciadv.abc2992/DC1

Submitted 16 April 2020
Accepted 26 May 2020
Published First Release 12 June 2020
10.1126/sciadv.abc2992

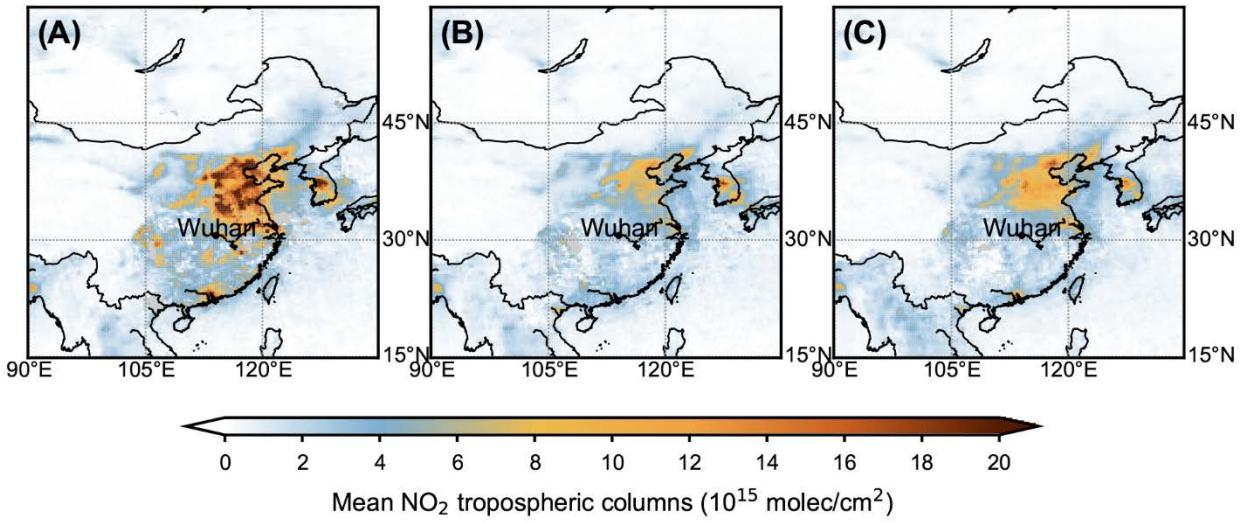

Fig. 1. Average OMI tropospheric NO_2 vertical column densities over China in 2020. (A) -20 to -1, (B) 0-19, and (C) 20-39 days relative to the 2020 Lunar New Year.

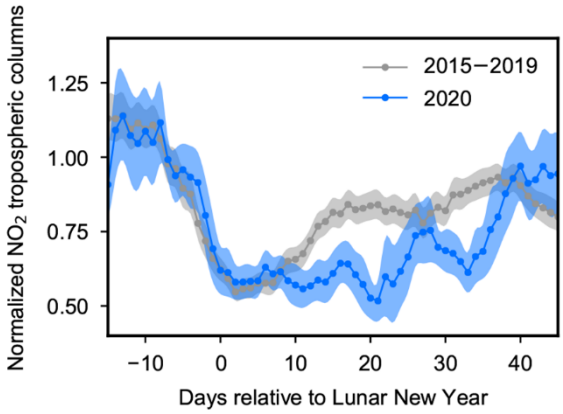

Fig. 2. Daily variations in 7-day moving averages of OMI NO_2 TVCDs over China. Shading shows standard error of the mean. Points are plotted at the midpoint of the 7-day moving average. Values are normalized to the mean of the pre period. Note that we account for the annually varying dates of the Lunar New Year.

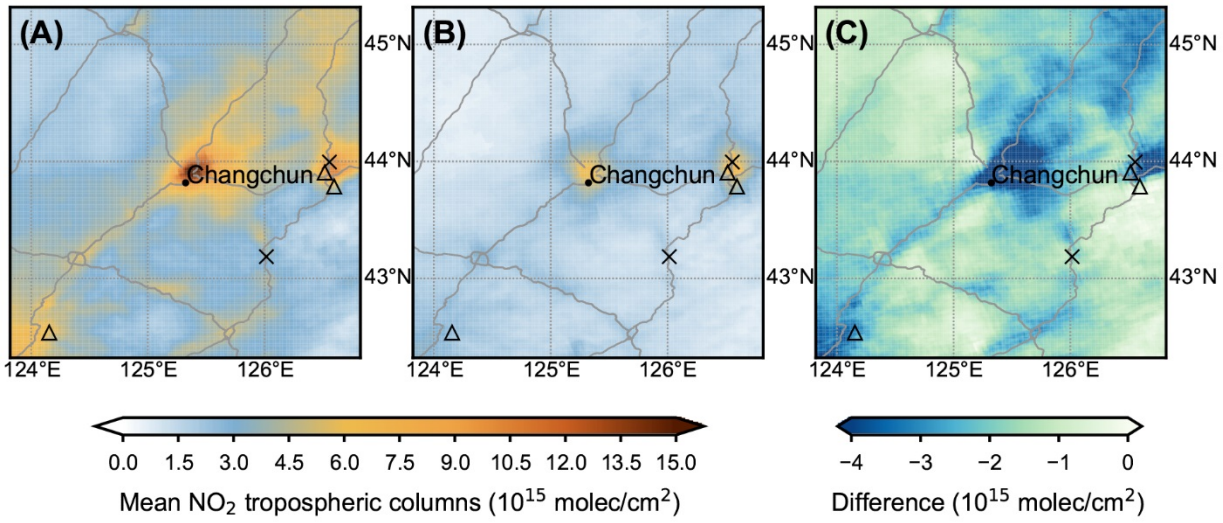

Fig. 3. Average TROPOMI NO_2 TVCD over Changchun, China (black dot) for 20 days. (A) Prior to **(B)** after the 2020 Lunar New Year, and **(C)** their difference. The locations of large power plants and other industrial plants are indicated by triangle and x, respectively. The lines show China National Highways.

Table 1. Effects of the government policies on NO_2 tropospheric vertical column density (TVCD).

	Outcome variable:		
	NO_2 TVCD (10^{15} molec/cm^2)		
	(1)	(2)	(3)
First case announced in province, β	-1.383**		-0.851*
	(0.409)		(0.401)
Lockdown of province, λ		-1.134***	-0.752***
		(0.226)	(0.158)
Average NO_2 TVCD 2015-2019, δ	0.0001	0.004	-0.002
	(0.019)	(0.018)	(0.019)
Constant, α	5.122	4.660	5.176
Number of observations	968	968	968
R^2	0.547	0.548	0.554
Adjusted R^2	0.533	0.534	0.539

Note. NO_2 TVCD is based on OMI. We use a fixed-effects model (Eqs. 1-3) with first case announced and lockdown coded as binary indicator variables. We control for the average 2015–2019 OMI NO_2 TVCDs to adjust for seasonal variation and include provinces' fixed-effects to adjust for geographical variation. The "Constant" term is the average province fixed-effect used as a baseline to compare the relative effect of the policy interventions. All standard errors (shown in parentheses) are clustered at the province level. * $p < 0.05$, ** $p < 0.01$, *** $p < 0.001$.

Abrupt decline in tropospheric nitrogen dioxide over China after the outbreak of COVID-19

Fei Liu, Aaron Page, Sarah A. Strode, Yasuko Yoshida, Sungyeon Choi, Bo Zheng, Lok N. Lamsal, Can Li, Nickolay A. Krotkov, Henk Eskes, Ronald van der A, Pepijn Veefkind, Pieternel F. Levelt, Oliver P. Hauser and Joanna Joiner

published online June 12, 2020

Science Advances (ISSN 2375-2548) is published by the American Association for the Advancement of Science, 1200 New York Avenue NW, Washington, DC 20005. The title *Science Advances* is a registered trademark of AAAS.